Biophysical Chemistry 203–204 (2015) 22–27

Contents lists available at ScienceDirect

Biophysical Chemistry

journal homepage: http://www.elsevier.com/locate/biophyschem

BII stability and base step flexibility of N_6-adenine methylated GATC motifs

Aleksandra Karolak, Arjan van der Vaart *

Department of Chemistry, University of South Florida, 4202 East Fowler Avenue CHE 205, Tampa, FL 33620, USA

HIGHLIGHTS

- Molecular dynamics simulations were performed on N_6-adenine methylated GATC motifs
- The GA step has the highest propensity for BII form when hemimethylated.
- The increased BII propensity correlates with increased stacking interactions.
- Flexibility of AT and TC steps is marginally affected by methylation.
- Possible implications for SeqA selectivity and binding are discussed.

GRAPHICAL ABSTRACT

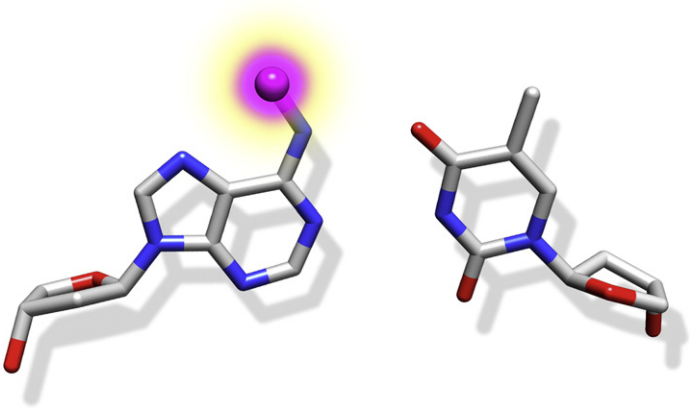

ARTICLE INFO

Article history:
Received 1 April 2015
Received in revised form 6 May 2015
Accepted 6 May 2015
Available online 12 May 2015

Keywords:
Adenine methylation
GATC sequence
Molecular dynamics
Free energy
DNA conformation

ABSTRACT

The effect of N_6-adenine methylation on the flexibility and shape of palindromic GATC sequences has been investigated by molecular dynamics simulations. Variations in DNA backbone geometry were observed, which were dependent on the degree of methylation and the identity of the bases. While the effect was small, more frequent BI to BII conversions were observed in the GA step of hemimethylated DNA. The increased BII population of the hemimethylated system positively correlated with increased stacking interactions between methylated adenine and guanine, while stacking interactions decreased at the TC step for the fully methylated strand. The flexibility of the AT and TC steps was marginally affected by methylation, in a fashion that was correlated with stacking interactions. The facilitated BI to BII conversion in hemimethylated strands might be of importance for SeqA selectivity and binding.

1. Introduction

A common epigenetic modification in prokaryotes and lower eukaryotes is N_6 methylation of adenine, which is important for transcription regulation, replication and repair [1–4]. In *Escherichia coli*, DNA adenine methyltransferase (Dam) methylates the N_6 position of adenine in GATC sequences [5–7]. Eleven of the ~19,000 GATC sites are clustered in the 245 base pair region of *E. coli* replication origin (*oriC*) [8]. While the adenines in most GATC sites are normally fully methylated (FMe), DNA exists in the hemimethylated form (HMe) after replication and before remethylation by Dam [3,9]. This HMe form is recognized by SeqA,

* Corresponding author. Tel.: +1 813 974 8762; fax: +1 813 974 3203.
E-mail address: avandervaart@usf.edu (A. van der Vaart).

http://dx.doi.org/10.1016/j.bpc.2015.05.001
0301-4622/

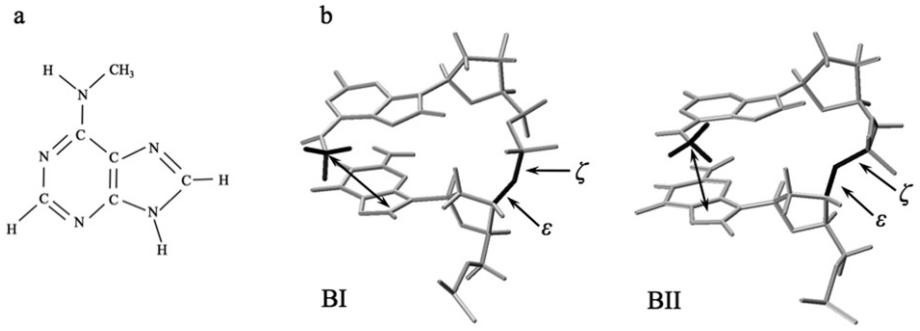

Fig. 1. DNA structure. (a) N_6-methylated adenine. (b) BI and BII conformations; ε and ζ dihedral angles are indicated. Also indicated are the distances between the carbon atom of the A_{18} methyl group (hydrogen in UMe) and the 5-membered ring of G_{17}, which were used in the stacking analyses.

which negatively regulates replication initiation and ensures that replication occurs only once during the cell cycle by binding HMe GATC at *oriC* [3,10,11].

Why SeqA preferentially binds HMe DNA has been studied in some detail. In addition to using electrostatic and hydrophobic interactions, DNA-binding proteins exploit subtle changes in local conformation and flexibility to recognize specific DNA sequences [12–17]. These properties are also used to identify epigenetic modifications since methylation increases local DNA hydrophobicity and may also affect the local conformation and elasticity of DNA [18,19]. In particular, N_6-adenine methylation decreases the melting temperature of DNA [19,20], may modulate DNA curvature [21], and induces undertwisting of the AT and overtwisting of the TC step in FMe and HMe GATC motifs [20,22]. It also affects DNA hydration [23] and stabilizes the BI conformation in TA repeats [24]. Structural studies of the SeqA–HMe complex showed that the only sequence specific contacts present are between the protein and the AT base pair within the GATC site [25]. Other studies implied the existence of additional factors that contribute to binding specificity since the mutation of C or G in the CG base pair of the GATC motif negatively influenced recognition [26]. NMR studies of unbound HMe DNA showed a compression of the major groove near the site of methylation [20], which was not observed in unbound FMe or UMe DNA [22]; this compression was similar to that observed in the SeqA–HMe complex [25]. Moreover, in the SeqA–HMe complex, the GC base pairs of the GATC motif were slightly opened [25], and unbound HMe DNA displayed faster base pair opening and closing rates of these base pairs than unbound FMe DNA [22]. While the difference in estimated barrier for opening between HMe and FMe was small (5.9 ± 1.7 kJ/mol), the observation that somewhat less energy was required for the opening of the GC base pairs in HMe than FMe suggested that this opening might be another driving force in the selective recognition of HMe [22].

Here we used molecular dynamics (MD) simulations to further investigate the structural and mechanical properties of the GATC motif of unbound UMe, HMe, and FMe DNA. Our study focused on two aspects. The first was the DNA backbone configuration since crystal structures of SeqA–DNA complexes [25,27,28] indicate the occurrence of the BII conformation at the AT step of the unmethylated chain and the GA step of the methylated chain. The DNA BI and BII form describe the relative position of the O3′ atom, which points towards the outside of the helix in BI and towards the inside of the helix in the BII form, and are defined with respect to the ε (C4′-C3′-O3′-P) and ζ (C3′-O3′-P-O5′) dihedral angles (Fig. 1). BI is present when $\varepsilon - \zeta < 0$ and BII when $\varepsilon - \zeta > 0$. BI is the common configuration for B-DNA, but BII is important for DNA–protein recognition since BII enhances exposure of DNA bases in the major groove [29–31]. The second aspect of our study focused on the flexibility of DNA, which is important for indirect readout. Given that the overall shape of DNA is mostly determined by roll and twist angles [32], we investigated the flexibility of roll and twist at the AT and TC steps and determined how this flexibility changed upon methylation. We also confirmed the effect of methylation on GC base pair opening by free energy simulations.

2. Materials and methods

MD simulations of 5′-GCGAGATCTGCG-3′ double-stranded DNA were performed, with adenine in the central GATC site in unmethylated and N_6-methylated forms (Fig. 1a). Both HMe, with methylation of the complementary strand, and FMe, with methylation of both the main and complementary strands, were simulated. Initial coordinates for the strands were obtained from Protein Data Bank (PDB) [33], entries 1OPQ (UMe) [20], 1UAB (HMe) [20], and 2KAL (FMe) [22]. In the HMe and FMe PDB files and the simulations, the N_6-adenine methyl groups were oriented *trans* to the adenine N_1 atom; this configuration also corresponds to that observed in SeqA–DNA complexes [25,27,28]. The sequence of the simulated strands is shown in Fig. 2; in HMe A_{18} of the complementary strand is methylated.

The DNA strands were solvated in a rectangular box of 150 mM NaCl solution of TIP3 water [34], with a minimum distance of 12 Å between the DNA and the edge of the box. After minimization, the systems were gradually heated from 120 K to 300 K over a period of 1 ns and equilibrated for 1.5 ns. During heating and equilibration, harmonic restraints with a force constant of 4.2 kJ/(mol Å^2) were used on the DNA heavy atoms. These restraints were subsequently released in steps of 500 ps each, using force constants of 2.1 and 0.4 kJ/(mol Å^2). Production runs started after a final unrestrained equilibration of 1 ns. These production runs consisted of 100 ns normal, unbiased MD; a total of three independent unbiased MD simulations starting from different random seeds for the heating were performed per system. Conformational analyses were performed to ensure that each of the systems was in steady state. In addition, one- and two-dimensional umbrella sampling simulations were performed. In one-dimensional umbrella sampling simulations [35], the N_4–O_6 distance between the C_8/G_{17} base pair was restrained to values between 1.5 and 5 Å, using windows of 0.5 Å and a

```
main          5′-G1 C2 G3 A4 G5 A6 T7 C8 T9 G10C11G12-3′
complementary 3′-C24G23C22T21C20T19A18G17A16C15G14C13-5′
```

Fig. 2. Simulated sequences, the GATC motif is underlined. A_{18} of the complementary strand is methylated in HMe; A_6 and A_{18} are methylated in FMe.

Table 1
Population (%) of BII forms in the GATC motif.

Step	UMe[a]	HMe, unmethylated	HMe, methylated	FMe[a]
GA	27.5 ± 3.7	28.8 ± 5.9	34.5 ± 3.9	27.6 ± 4.5
AT	1.4 ± 0.3	2.6 ± 1.4	1.4 ± 0.4	1.6 ± 0.8
TC	14.5 ± 1.6	11.8 ± 3.7	11.1 ± 2.5	14.4 ± 1.2

[a] Averaged values over both DNA strands.

Table 2
Populations (%) of mixed BI and BII states on DNA main and complementary strands at $A_6T_7/A_{18}T_{19}$ and $T_7C_8/G_{17}A_{18}$ steps.

	BI/BI	BI/BII	BII/BI	BII/BII
$A_6T_7/A_{18}T_{19}$				
UMe	98	1	1	0
HMe	97	1	2	0
FMe	95	3	2	0
$T_7C_8/G_{17}A_{18}$				
UMe	68	20	9	3
HMe	56	31	8	5
FMe	63	25	6	6

force constant of 4.2 kJ/(mol Å^2); each window was simulated for 5 ns. Two-dimensional umbrella sampling simulations were performed of the twist and roll angles of the central $A_6T_7/A_{18}T_{19}$ and $T_7C_8/G_{17}A_{18}$ base steps [36]. In these simulations, the base step parameters and their analytical derivatives were calculated in a highly efficient manner that avoids the use of overlays [36], as was previously done in a similar manner for roll only [37–40]. The simulations were performed in 99 windows that were distributed between 20° and 60° for twist and −20° and 30° for roll, using a step size of 5° and a force constant of 2.1 kJ/(mol deg^2). After restrained heating and 1 ns equilibration, each window was sampled for 2 ns. Overlap of distributions in the umbrella sampling simulations was verified visually, and free energy surfaces were calculated with the weighted histogram analysis method [41,42] using a bin size of 0.1 Å for the N_4–O_6 distance and 1° for twist and roll. Total production times were 0.9 μs for the unbiased MD, 120 ns for the one-dimensional, and 1.2 μs for the two-dimensional umbrella sampling simulations. All simulations were performed with the CHARMM program [43], and the CHARMM 36 force field [44], which was optimized to reproduce BI/BII populations [44]. The simulations used a time step of 2 fs, SHAKE to constrain bonds with hydrogen atoms [45], the Nosé–Hoover thermostat for temperature control [46], and the particle mesh Ewald method [47] for long-range electrostatic interactions. Trajectories were analyzed with VMD [48], PyMol [49], 3DNA [50], and CHARMM [43]; error analyses were performed by block averaging. The two-dimensional umbrella sampling simulations were run using computing resources at XSEDE [51] and USF Research Computing (RC), at a cost of 256 central processing unit (CPU) hours per ns, and 360 CPU hours per ns of simulation, respectively. The one-dimensional umbrella sampling simulations and the independent unbiased simulations took 400 CPU hours per ns at USF RC; several of these were run with CHARMM-OpenMM [52] using NVIDIA K20 graphical processing units (GPUs) at a cost of 1 GPU hour per ns.

3. Results and discussion

The BII populations of all steps of the central GATC motif of the UMe, HMe, and FMe strands are shown in Table 1. Both the GA and the TC steps showed significant amounts of BII conformations, while the AT step was almost purely BI for all chains. Steps involving two pyrimidines are thought to visit the BII conformation rarely [31], but here the TC step of all systems populated the BII form by more than 10%, with a slightly higher percentage in the UMe and FMe systems. The most significant variations in BII populations were observed at the GA step, where the HMe system showed the largest BII population on the methylated strand. This population for the methylated strand was 7% higher than UMe and FMe, and 6% higher than in the unmethylated HMe strand. While small, this difference is of interest, since the GA step of the methylated strands is in the BII form in SeqA–DNA complexes [25,27,28], and even small differences in the inherent propensity to adopt bound-like geometries will aid selectivity and binding [53,54].

Further analyses revealed a correlation between the BI/BII populations and stacking interactions. In Fig. 3 the distance between A_{18} and G_{17} is graphed versus the ε–ζ value of the $G_{17}A_{18}$ step. For UMe, this distance corresponds to the H_6 atom of A_{18} and the 5-membered ring of G_{17}, while for HMe and FMe, the distance is between the carbon methyl atom of A_{18} and the 5-membered ring of G_{17} (shown in Fig. 1b). Fig. 3 shows that the BII conformation is accompanied by much tighter stacking in both HMe and FMe. While the A_{18}-G_{17} distance fluctuates strongly in the BII conformation of UMe, the distance is locked to smaller values in BII of HMe and FMe. The strongest stacking interactions in BII are observed in HMe, which helps explain that the largest fraction of BII was observed for the GA step of HMe.

In the BI form, the A_{18}-G_{17} distance increases in FMe (Fig. 3c), which is due to hydrophobic interactions between the methyl groups of A_6 and A_{18}. Our data indicate that hydrophobic interactions might also be responsible for the low occurrence of BII at the AT step. Structural analyses showed that interactions between the methyl groups of mA_6 and mA_{18} and the methyl groups of the adjacent thymine within the AT step weaken stacking interactions in the BII form. The thymine and adenine methyl groups are both located in the major groove, and the decrease of TA stacking within the step disfavors the BII transition.

The occurrences of mixed BI/BII states for the $A_6T_7/A_{18}T_{19}$ and $T_7C_8/G_{17}A_{18}$ steps are listed in Table 2. Since the AT steps sampled BII only marginally, BI/BI was predominant and there was a low fraction of BI/BII and BII/BI. At this step, twist values were around 30°. The populations of BI/BII and BII/BI increased at the $T_7C_8/G_{17}A_{18}$ step, which was accompanied by elevated values of twist in all systems (41° for UMe,

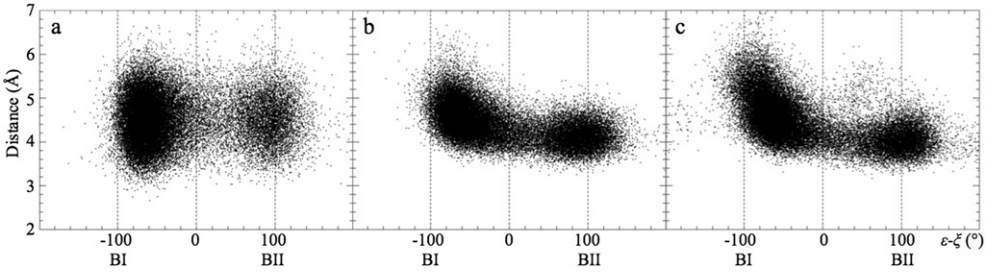

Fig. 3. Correlation between stacking interactions and ε–ζ value for UMe (a), HMe (b), and FMe (c). Distance is measured between the carbon atom of methyl group on A_{18} (hydrogen in UMe) and the 5-membered ring of G_{17}, as illustrated in Fig. 1.

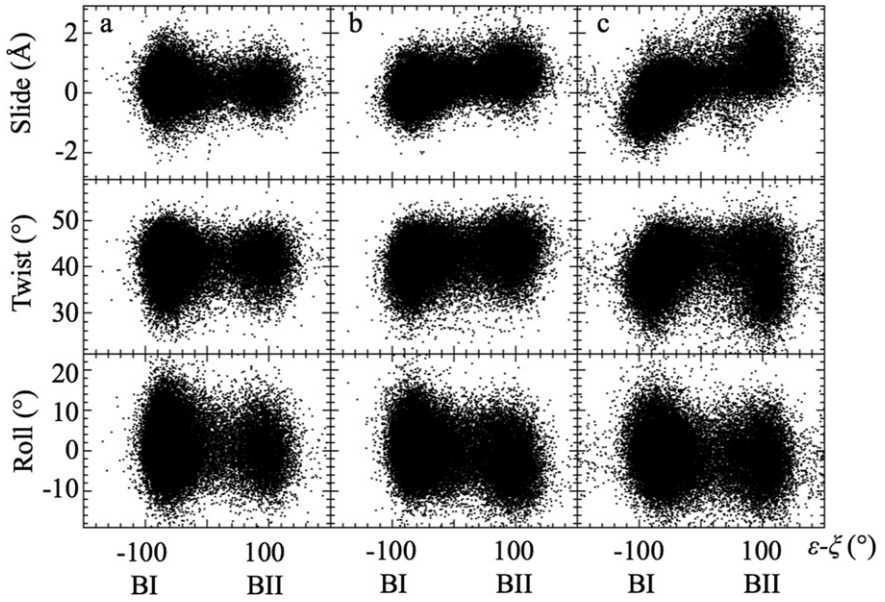

Fig. 4. Correlation between slide, twist, and roll and ε–ζ values at the $T_7C_8/G_{17}A_{18}$ steps for UMe (a), HMe (b), and FMe (c).

42° for HMe, 40° for FMe). A correlation between twist and mixed state populations has been observed in other sequences before [20,31,55]. HMe had the highest value of twist and the highest population of mixed BI/BII states (39%) at the $T_7C_8/G_{17}A_{18}$ step. In addition to the correlation with twist, the BII population at the $T_7C_8/G_{17}A_{18}$ steps was strongly correlated with slide (Fig. 4). Weaker positive correlations were observed with shift, and to a lesser degree tilt, while the correlation with roll was negative. The latter is a result of the negative correlation between twist and roll that stems from geometrical effects [32,36,56–58]. The twist-roll correlation was particularly evident for the BII form of HMe, which had the highest twist and lowest roll.

Whereas slide for UMe system was ~0.23 Å in BI and ~0.24 Å in BII form, the methylation of adenine altered slide in a strongly correlated fashion. The higher the degree of methylation, the lower the value of slide in BI form and the higher its value in BII. For FMe, this led to an average negative slide (-0.09 Å) in the BI form, and large positive (0.93 Å) in BII. Since nonoptimal values of slide may lead to the loss of stacking interactions [59], this change in slide may help explain the decreased stability of FMe.

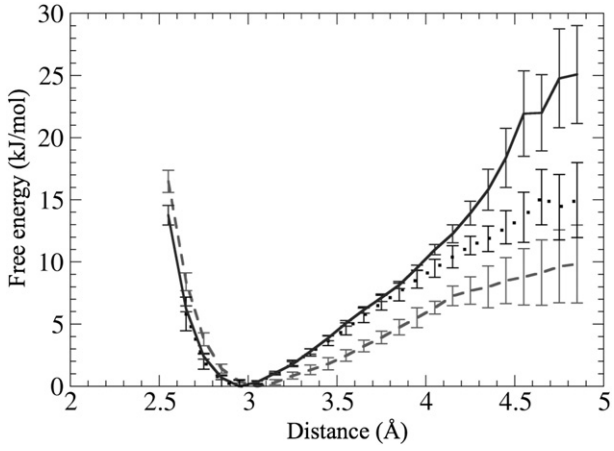

Fig. 5. Free energy as a function of the N_4–O_6 distance in the C_8/G_{17} base pair for UMe (solid line), HMe (dashed line), and FMe (dotted line).

One-dimensional umbrella sampling simulations of the N_4–O_6 distance at base pair C_8/G_{17} confirmed that base pair opening is slightly less energy costly for HMe. The free energy of opening is shown as a function of distance in Fig. 5. None of the curves is symmetric around the minima because of steric clashes at close proximity of the bases. In HMe the equilibrium, N_4–O_6 distance is slightly higher (3.05 Å) than in UMe and FMe (2.95 Å). Moreover, while the cost of opening is similar in UMe and FMe, this energy is nearly halved in HMe. The similar behavior of FMe and UMe implies that presence of second methyl group counteracts the effect of hemimethylation. Although the effect is subtle, HMe will sample opening distances close to that observed in the SeqA–DNA complex more frequently than UMe and FMe.

Two-dimensional free energy surfaces as a function of twist and roll for the $A_6T_7/A_{18}T_{19}$ and $T_7C_8/G_{17}A_{18}$ steps are shown in Fig. 6; the twist-roll covariance matrices are shown in Table 3. The free energy surfaces show undertwisting of the $A_6T_7/A_{18}T_{19}$ step and overtwisting of the $T_7C_8/G_{17}A_{18}$ steps. The basins stretch along the anti-diagonal direction; this negative correlation between changes in twist and roll is commonly observed in DNA [32,36,56–58]. The HMe $A_6T_7/A_{18}T_{19}$ step is slightly more flexible in twist and roll than UMe and FMe, while UMe is somewhat more flexible in twist and stiffer in roll than FMe. The roll flexibility of the $T_7C_8/G_{17}A_{18}$ step strongly correlates with $G_{17}A_{18}$ stacking (Fig. 3). The highest flexibility is observed for UMe, which had the least amount of $G_{17}A_{18}$ stacking, while HMe had the largest stacking interactions and is least flexible. In a similar manner, the twist flexibility at the $T_7C_8/G_{17}A_{18}$ step is also correlated with the stacking flexibility, but this correlation is less pronounced than for roll. The methylated systems show slightly stiffer twists than the unmethylated systems, and the twist of HMe is the least flexible.

4. Conclusion

In conclusion, MD simulations of UMe, HMe, and FMe GATC sequences showed differences in BI/BII populations. The methylated strand of HMe showed larger BII populations of the GA step than UMe and FMe. The small increase in BII population was correlated with an increase in stacking interactions in HMe. In FMe, a large decrease in slide was observed when the TC step was BI and a large increase in slide when it was BII, indicating a decrease of stacking interactions. Given that the GA step of the methylated strands is in BII form in SeqA–DNA

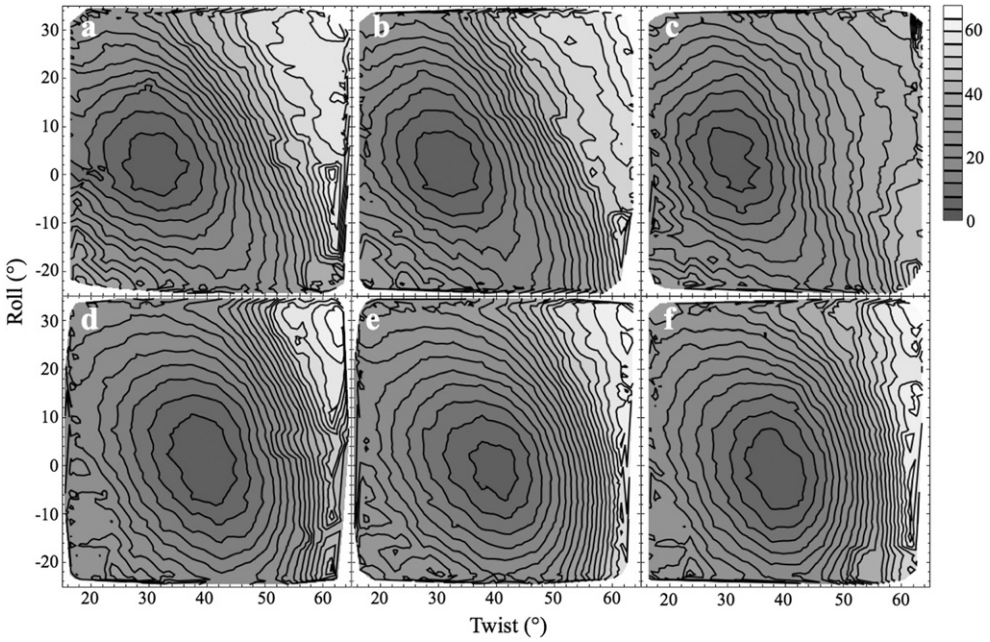

Fig. 6. Free energy surfaces (in kJ/mol) calculated as a function of twist and roll at $A_6T_7/A_{18}T_{19}$ step for UMe (a), HMe (b) and FMe (c), and for $T_7C_8/G_{17}A_{18}$ step for UMe (d), HMe (e), and FMe (f).

Table 3
Twist-roll covariance matrices from data points up to 17 kJ/(mol deg^2) on the free energy surfaces.

Step	UMe	HMe	FMe
$A_6T_7/A_{18}T_{19}$	$\begin{pmatrix} 56 & -24 \\ -24 & 92 \end{pmatrix}$	$\begin{pmatrix} 62 & -46 \\ -46 & 128 \end{pmatrix}$	$\begin{pmatrix} 43 & -24 \\ -24 & 102 \end{pmatrix}$
$T_7C_8/G_{17}A_{18}$	$\begin{pmatrix} 51 & -25 \\ -25 & 115 \end{pmatrix}$	$\begin{pmatrix} 44 & -17 \\ -17 & 82 \end{pmatrix}$	$\begin{pmatrix} 46 & -17 \\ -17 & 99 \end{pmatrix}$

complexes [25,27,28], the small difference in BII populations might be exploited by SeqA to facilitate the recognition of the hemimethylated strand. Simulations confirmed that the opening of the GC base pair is more facile in HMe and showed slight differences in the ease of twist and roll deformations at the AT and TC step of the UMe, HMe, and FMe systems. These differences in stiffness were well correlated with relative stacking interactions.

Acknowledgments

This work was supported by NSF CAREER Award No. CHE-1007816. Computer time was partly provided by USF Research Computing. This work also used the Extreme Science and Engineering Discovery Environment (XSEDE), which is supported by National Science Foundation grant number ACI-1053575. Trajectories will be made available upon request.

References

[1] F. Vanyushin, Methylation of adenine residues in DNA of eukaryotes, Mol. Biol. 39 (2005) 557–566.
[2] S. Hattman, DNA-[adenine] methylation in lower eukaryotes, Biochemistry (Moscow) 70 (2005) 550–558.
[3] D. Wion, J. Casadesus, N-6-methyl-adenine: an epigenetic signal for DNA–protein interactions, Nat. Rev. Microbiol. 4 (2006) 183–192.
[4] D. Ratel, J.L. Ravanat, F. Berger, D. Wion, N6-methyladenine: the other methylated base of DNA, Bioessays 28 (2006) 309–315.
[5] G.E. Geier, P. Modrich, Recognition sequence of the dam methylase of *Escherichia-coli*-K12 and mode of cleavage of Dpn-I endonuclease, J. Biol. Chem. 254 (1979) 1408–1413.
[6] A. Jeltsch, Beyond Watson and Crick: DNA methylation and molecular enzymology of DNA methyltransferases, Chembiochem 3 (2002) 275–293.
[7] A. Jeltsch, Beyond Watson and Crick: DNA methylation and molecular enzymology of DNA methyltransferases (Vol 3, pg 274, 2002), Chembiochem 3 (2002) 382-382.
[8] A. Henaut, T. Rouxel, A. Gleizes, I. Moszer, A. Danchin, Uneven distribution of GATC motifs in the *Escherichia coli* chromosome, its plasmids and its phages, J. Mol. Biol. 257 (1996) 574–585.
[9] G.B. Ogden, M.J. Pratt, M. Schaechter, The replicative origin of the *Escherichia-coli* chromosome binds to cell-membranes only when hemimethylated, Cell 54 (1988) 127–135.
[10] M. Lu, J.L. Campbell, E. Boye, N. Kleckner, Seqa—a negative modulator of replication initiation in *Escherichia-coli*, Cell 77 (1994) 413–426.
[11] S. Kang, H. Lee, J.S. Han, D.S. Hwang, Interaction of SeqA and Dam methylase on the hemimethylated origin of *Escherichia coli* chromosomal DNA replication, J. Biol. Chem. 274 (1999) 11463–11468.
[12] R. Rohs, X. Jin, S.M. West, R. Joshi, B. Honig, R.S. Mann, Origins of specificity in protein–DNA recognition, Annu. Rev. Biochem. 79 (2010) 233–269.
[13] C.O. Pabo, R.T. Sauer, Protein–DNA recognition, Annu. Rev. Biochem. 53 (1984) 293–321.
[14] A. Sarai, H. Kono, Protein–DNA recognition patterns and predictions, Annu. Rev. Biophys. Biomol. Struct. 34 (2005) 379–398.
[15] R.E. Harrington, DNA curving and bending in protein DNA recognition, Mol. Microbiol. 6 (1992) 2549–2555.
[16] R.K. Allemann, M. Egli, DNA recognition and bending, Chem. Biol. 4 (1997) 643–650.
[17] A. van der Vaart, Coupled binding–bending–folding: the complex conformational dynamics of protein–DNA binding studied by atomistic molecular dynamics simulations, Biochim. Biophys. Acta Gen. Subj. 1850 (2015) 1091–1098.
[18] D. Nathan, D.M. Crothers, Bending and flexibility of methylated and unmethylated EcoRI DNA, J. Mol. Biol. 316 (2002) 7–17.
[19] J.D. Engel, P.H.V. Hippel, Effects of methylation on stability of nucleic-acid conformations—studies at polymer level, J. Biol. Chem. 253 (1978) 927–934.
[20] S.H. Bae, H.K. Cheong, C. Cheong, S.H. Kang, D.S. Hwang, B.S. Choi, Structure and dynamics of hemimethylated GATC sites implications for DNA-SeqA recognition, J. Biol. Chem. 278 (2003) 45987–45993.
[21] P. Polaczek, K. Kwan, J.L. Campbell, GATC motifs may alter the conformation of DNA depending on sequence context and N-6-adenine methylation status: possible implications for DNA–protein recognition, Mol. Gen. Genet. 258 (1998) 488–493.
[22] J. Bang, S.-H. Bae, C.-J. Park, J.-H. Lee, B.-S. Choi, Structural and dynamics study of DNA dodecamer duplexes that contain un-, hemi-, or fully methylated GATC sites, J. Am. Chem. Soc. 130 (2008) 17688–17696.
[23] S. Shanak, V. Helms, Hydration properties of natural and synthetic DNA sequences with methylated adenine or cytosine bases in the R.DpnI target and BDNF promoter studied by molecular dynamics simulations, J. Chem. Phys. 141 (2014).
[24] F.R. Wibowo, M. Trieb, C. Rauch, B. Wellenzohn, K.R. Liedl, The N6-methyl group of adenine further increases the BI stability of DNA compared to C5-methyl groups, J. Phys. Chem. B 109 (2005) 557–564.
[25] A. Guarne, Q.H. Zhao, R. Ghirlando, W. Yang, Insights into negative modulation of *E-coli* replication initiation from the structure of SeqA–hemimethylated DNA complex, Nat. Struct. Biol. 9 (2002) 839–843.
[26] T. Brendler, S. Austin, Binding of SeqA protein to DNA requires interaction between two or more complexes bound to separate hemimethylated GATC sequences, EMBO J. 18 (1999) 2304–2310.
[27] N. Fujikawa, H. Kurumizaka, O. Nureki, Y. Tanaka, M. Yamazoe, S. Hiraga, S. Yokoyama, Structural and biochemical analyses of hemimethylated DNA binding by the SeqA protein, Nucleic Acids Res. 32 (2004) 82–92.

[28] Y.S. Chung, T. Brendler, S. Austin, A. Guarne, Structural insights into the cooperative binding of SeqA to a tandem GATC repeat, Nucleic Acids Res. 37 (2009) 3143–3152.
[29] D. Djuranovic, B. Hartmann, DNA fine structure and dynamics in crystals and in solution: the impact of BI/BII backbone conformations, Biopolymers 73 (2004) 356–368.
[30] J.S. Lamoureux, J.N.M. Glover, Principles of protein–DNA recognition revealed in the structural analysis of Ndt80-MSE DNA complexes, Structure 14 (2006) 555–565.
[31] A. Madhumalar, M. Bansal, Sequence preference for BI/II conformations in DNA: MD and crystal structure data analysis, J. Biomol. Struct. Dyn. 23 (2005) 13–27.
[32] R.E. Dickerson, DNA bending: the prevalence of kinkiness and the virtues of normality, Nucleic Acids Res. 26 (1998) 1906–1926.
[33] H.M. Berman, J. Westbrook, Z. Feng, G. Gilliland, T.N. Bhat, H. Weissig, I.N. Shindyalov, P.E. Bourne, The protein data bank, Nucleic Acids Res. 28 (2000) 235–242.
[34] W. Jorgensen, J. Chandrasekar, J. Madura, R. Impey, M. Klein, Comparison of simple potential functions for simulating liquid water, J. Chem. Phys. 79 (1983) 926–935.
[35] G.M. Torrie, J.P. Valleau, Non-physical sampling distributions in Monte-Carlo free-energy estimation—umbrella sampling, J. Comput. Phys. 23 (1977) 187–199.
[36] A. Karolak, A. van der Vaart, Enhanced sampling simulations of DNA step parameters, J. Comput. Chem. 35 (2014) 2297–2304.
[37] J. Spiriti, H. Kamberaj, A.M.R. de Graff, M.F. Thorpe, A. van der Vaart, DNA bending through large angles is aided by ionic screening, J. Chem. Theory Comput. 8 (2012) 2145–2156.
[38] J. Spiriti, A. van der Vaart, DNA bending through roll angles is independent of adjacent base pairs, J. Phys. Chem. Lett. 3 (2012) 3029–3033.
[39] J. Spiriti, A. van der Vaart, DNA binding and bending by Sac7d is stepwise, ChemBioChem 14 (2013) 1434–1437.
[40] Y.H. Chung, A. van der Vaart, RevErba preferentially deforms DNA by induced fit, ChemBioChem 15 (2014) 643–646.
[41] A.M. Ferrenberg, R.H. Swendsen, Optimized Monte-Carlo data-analysis, Phys. Rev. Lett. 63 (1989) 1195–1198.
[42] A. Grossfield, An implementation of WHAM: the weighted histogram analysis method, http://membrane.urmc.rochester.edu/Software/WHAM/WHAM.html 2010.
[43] B.R. Brooks, C.L. Brooks III, A.D. MacKerell Jr., L. Nilsson, R.J. Petrella, B. Roux, Y. Won, G. Archontis, C. Bartels, S. Boresch, A. Caflisch, L. Caves, Q. Cui, A.R. Dinner, M. Feig, S. Fischer, J. Gao, M. Hodoscek, W. Im, K. Kuczera, T. Lazaridis, J. Ma, V. Ovchinnikov, E. Paci, R.W. Pastor, C.B. Post, J.Z. Pu, M. Schaefer, B. Tidor, R.M. Venable, H.L. Woodcock, X. Wu, W. Yang, D.M. York, M. Karplus, CHARMM: the biomolecular simulation program, J. Comb. Chem. 30 (2009) 1545–1614.
[44] K. Hart, N. Foloppe, C.M. Baker, E.J. Denning, L. Nilsson, A.D. MacKerell, Optimization of the CHARMM additive force field for DNA: improved treatment of the BI/BII conformational equilibrium, J. Chem. Theory Comput. 8 (2012) 348–362.
[45] J.P. Ryckaert, G. Ciccotti, H.J.C. Berendsen, Numerical integration of the Cartesian equations of motion of a system with constraints: molecular dynamics of n-alkanes, J. Comput. Phys. 23 (1977) 327–341.
[46] W.G. Hoover, Canonical dynamics: equilibrium phase-space distributions, Phys. Rev. A 31 (1985) 1695–1697.
[47] T. Darden, D. York, L. Pedersen, Particle mesh Ewald: an N log(N) method for Ewald sums in large systems, J. Chem. Phys. 98 (1993) 10089–10092.
[48] W. Humphrey, A. Dalke, K. Schulten, VMD: visual molecular dynamics, J. Mol. Graph. 14 (1996) 33-&.
[49] W.L. Delano, The PyMol Molecular Graphics System, Version 1.3, Schrödinger, LLC.
[50] X.J. Lu, W.K. Olson, 3DNA: a versatile, integrated software system for the analysis, rebuilding and visualization of three-dimensional nucleic-acid structures, Nat. Protoc. 3 (2008) 1213–1227.
[51] J. Towns, T. Cockerill, M. Dahan, I. Foster, K. Gaither, A. Grimshaw, V. Hazlewood, S. Lathrop, D. Lifka, G.D. Peterson, R. Roskies, J.R. Scott, N. Wilkins-Diehr, XSEDE: accelerating scientific discovery, Comput. Sci. Eng. 16 (2014) 62–74.
[52] P. Eastman, M.S. Friedrichs, J.D. Chodera, R.J. Radmer, C.M. Bruns, J.P. Ku, K.A. Beauchamp, T.J. Lane, L.P. Wang, D. Shukla, T. Tye, M. Houston, T. Stich, C. Klein, M.R. Shirts, V.S. Pande, OpenMM 4: a reusable, extensible, hardware independent library for high performance molecular simulation, J. Chem. Theory Comput. 9 (2013) 461–469.
[53] P. Csermely, R. Palotai, R. Nussinov, Induced fit, conformational selection and independent dynamic segments: an extended view of binding events, Trends Biochem. Sci. 35 (2010) 539–546.
[54] R. Bryn Fenwick, S. Esteban-Martin, X. Salvatella, Understanding biomolecular motion, recognition, and allostery by use of conformational ensembles, Eur. Biophys. J. Biophys. 40 (2011) 1339–1355.
[55] T. Drsata, M. Kara, M. Zacharias, F. Lankas, Effect of 8-oxoguanine on DNA structure and deformability, J. Phys. Chem. B 117 (2013) 11617–11622.
[56] W.K. Olson, A.A. Gorin, X.-J. Lu, L.M. Hock, V.B. Zhurkin, DNA sequence-dependent deformability deduced from protein–DNA crystal complexes, Proc. Natl. Acad. Sci. U. S. A. 95 (1998) 11163–11168.
[57] S. Kannan, K. Kohlhoff, M. Zacharias, B-DNA under stress: over-and untwisting of DNA during molecular dynamics simulations, Biophys. J. 91 (2006) 2956–2965.
[58] A. Perez, C.L. Castellazzi, F. Battistini, K. Collinet, O. Flores, O. Deniz, M.L. Ruiz, D. Torrents, R. Eritja, M. Soler-Lopez, M. Orozco, Impact of methylation on the physical properties of DNA, Biophys. J. 102 (2012) 2140–2148.
[59] H.O. Bertrand, T. Ha-Duong, S. Fermandjian, B. Hartmann, Flexibility of the B-DNA backbone: effects of local and neighbouring sequences on pyrimidine-purine steps, Nucleic Acids Res. 26 (1998) 1261–1267.